Proceedings of ESDA2002:
6th Biennial Conference on Engineering Systems Design and Analysis
Istanbul, Turkey, July 8-11, 2002

ESDA 2002/DES-005

IMPACT OF TOOTH PROFILE MODIFICATIONS ON THE TRANSMISSION ERROR EXCITATION OF HELICAL GEAR PAIRS

Parag Wagaj (*)
Research Associate
Center for Gear Research
The University of Toledo
Toledo, OH 43606, USA

Ahmet Kahraman
Associate Professor and Director
Center for Gear Research
The University of Toledo
Toledo, OH 43606, USA
E-mail: akahrama@eng.utoledo.edu

Abstract

In this study, a nonlinear finite element contact mechanics model of a parallel axis gear pair is employed to study the impact of intentional tooth flank modifications on the static motion transmission error of the gear pair. An experimental study is performed for the validation of the model predictions. The validated model is then employed to investigate the impact of both two-dimensional (2D) and three-dimensional (3D) tooth flank modifications on the transmission error excitation. In case of 2D modifications, a parameter set that includes the magnitude, extent, and type (linear or quadratic) of involute tip modifications and lead crown is considered. For 3D modifications, parameters defining both "bias-in" and "bias-out" type of modifications are included. The combined influence of modification parameters and load transmitted on the resultant transmission error excitation is quantified.

Nomenclature

a	Magnitude of 2D tip of root modification
A_i	i-th gear mesh harmonic component of $\varepsilon(t)$
b	Magnitude of 3D modification
h	Magnitude of 2D lead modification
P	Modification parameter set
$\mathbf{q}$	Position vector of a reference point on the matching interface
r	Gear radius
$\mathbf{r}$	Position vector of a surface point
t	Time
T	Torque transmitted
T_d	Design torque
u	Inward normal component of the displacement vector
α	Starting roll angle of a 2D profile modification
β	Starting roll angle of a 3D modification in profile direction
$\varepsilon(t)$	Static transmission error
λ	Length of a 3D modification in lead direction
θ	Gear rotation angle
Ω	Nominal angular velocity

Superscripts:

fe	Finite element
i	Gear index ($i = p, g$)
g	Gear
p	Pinion
si	Surface integral

Subscripts:

a	Alternating component
d	Deflection component
f	Geometric deviation component

1 Introduction

Dynamic modeling of gear pairs has attracted large number of investigators over last 40 years [1]. Any attempt in reducing noise generated by a gear pair and in improving the durability of the system requires a sound understanding of the behavior of the system under dynamic conditions. A dynamic model with all essential features of the actual physical system is required for this purpose. This way, not only the vibratory behavior of

(*) Currently with M&M Precision Systems Corp, Dayton, OH.

a gear pair leading to gear noise and dynamic stressses can be described, but also the key parameters can be identified and optimized for the most favorable gear dynamics behavior.

Several recent published studies on gear dynamics [2-11] point out that a gear pair behaves as a non-linear, time-varying system with a rather complex excitation mechanism formed by a number of parametric, internal and external excitations. Considering a gear pair formed by gears *p* (driving) and *g* (driven), three types of excitations were reported to exist [4]. The first one is a parametric excitation due to the periodically time-varying gear mesh stiffness. It has been shown experimentally [6, 12] and analytically [11] that the amount of fluctuation of the mesh stiffness about its average value is dictated by the contact ratio (a gear pair design parameter representing average number of tooth pairs in contact). For spur gear pairs, any integer valued contact ratio, say one or two, eliminates largely this parametric excitation reducing overall vibration amplitudes and avoiding the parametric instability regions completely [6]. Secondly, an external excitation is present mainly due to low-frequency torque fluctuations originated by the prime mover, (engine, turbine, etc.) asserting very limited influence on the gear whine while it can be critical for rattling of unloaded gear pairs. Finally, the third type of excitation $\varepsilon(t)$ is an internal displacement excitation applied at the gear mesh between the teeth in order to represent deviations from the perfect involute profile due to manufacturing errors and/or intentional modifications, and quasi-static tooth deflections. It is also known as the *loaded static transmission error*. In lumped mass dynamic models, $\varepsilon(t)$ was introduced as a displacement excitation at the gear mesh interface while deformable body dynamic models include $\varepsilon(t)$ implicitly [11]. In either case, reducing $\varepsilon(t)$ was shown to have the positive impact in the dynamic response of a spur gear pair resulting in reduced gear whine.

The rotational angle of gear-*i* ($i = p, g$) $\theta^i(t)$ can be written as the sum of a nominal rotation angle $\Omega^i t$ and an alternating component $\theta_a^i(t)$ where *t* represents the real time and Ω^i is the mean rotational velocity, i.e. $\theta^i(t) = \Omega^i t + \theta_a^i(t)$. Static transmission error along the line of action is then defined mathematically as

$$\varepsilon(t) = r^p \theta_a^p(t) + r^g \theta_a^g(t). \quad (1)$$

where r^p and r^g are the base circle radii. In physical terms, $\varepsilon(t)$ has two components, a geometric deviation component $\varepsilon_f(t)$ representing the unavoidable tooth flank manufacturing errors or intentional modifications and a component representing the quasi-static tooth deflections $\varepsilon_d(t)$

$$\varepsilon(t) = \varepsilon_f(t) + \varepsilon_d(t). \quad (2)$$

Under no load, the transmission error is formed solely by the geometric deviation component. Hence, a perfect involute gear pair under no load would have a zero transmission error. On the other hand, gear teeth in contact interface will deflect under load resulting in a certain $\varepsilon_d(t)$ even if the gears are perfect. For the most general case, gears have manufacturing errors and must carry a certain amount of load. Therefore, both components of $\varepsilon(t)$ in eq. (2) are equally relevant in real life powertrain gearing applications.

One commonly practiced idea has been to introduce a geometric deviation component $\varepsilon_f(t)$ that is equal to $\varepsilon_d(t)$ in magnitude but opposite in deflection, $\varepsilon_f(t) \approx -\varepsilon_d(t)$ so that $\varepsilon(t) \approx 0$ eliminating the transmission error excitation all together. This is done by modifying a gear tooth profile by introducing intentional deviations from a pure involute tooth flank surface through the final manufacturing process. This often amounts to removal of additional material from the tooth surface beyond the perfect involute profile. In eq. (2), $\varepsilon_f(t)$ includes modifications as well as other manufacturing errors. While their primary function is to reduce $\varepsilon(t)$, these tooth surface modifications also help in smoothening the entry and exit of a gear tooth to and from the meshing zone, and in compensating for mounting errors and deflections of the support structures such as shaft misalignments and shaft, bearing and case deflections.

Two types of involute tooth flank modifications have been in use for spur and helical gears. The first type is a two dimensional modification where the tooth flank is modified in involute (root to tip) and lead (side to side) directions independently. In involute direction, the profile defined by the perfect involute curve is altered by removing material at the tip (tip modification or tip relief) and/or root (root modification or root relief) as defined in Fig. 1(a). The magnitude at the tip a_t and the gear roll angle at the start of the tip relief α_t define the boundaries of the tip relief. Between these two points the profile typically follows a linear or quadratic trajectory. Similarly, the magnitude a_r and the starting roll angle α_r define the limits of a linear or quadratic root modification. 2D modifications in lead direction are typically given in the form of a "lead crown" that is tangent to the purely involute surface in the mid-plane of the gear and varies symmetrically in a quadratic manner in both directions reaching a magnitude of *h* at both sides of the gear tooth as shown in Fig. 1(a). Hence, a five parameter set P_{2D}^i defines 2D modifications of a gear *i*

$$P_{2D}^i \in \{a_t^i, \alpha_t^i, a_r^i, \alpha_r^i, h^i\} \quad (3)$$

resulting in a 10 parameter set $P_{2D} \in P_{2D}^p \cup P_{2D}^g$ for a pair formed by gears *p* and *g*. As seen in Fig. 1(a), profile modifications (tip and root relief) remain unchanged in the lead direction. Similarly, the modified shape in lead direction does not change in the involute direction. A close look at the directionality of typical contact lines of a spur gear pair should reveal that the lead crown of 2D modifications is applied in a direction parallel to the contact lines, and the profile modifications are perpendicular to the contact lines. Hence, the lead modifications here have the sole duty of preventing excessive loading near the faces of gears due to potential shaft misalignments while the profile modifications are devoted to controlling loaded transmission error excitation $\varepsilon(t)$ of a spur gear pair. It was shown in previous experimental and theoretical investigations that such modifications could be

designed to minimize $\varepsilon(t)$ of a spur gear pair at given *design load* [5,9,13,14].

In case of a helical gear pair, the contact lines are skewed by a certain amount due to the helix angle. Therefore, neither lead nor involute corrections of 2D modifications lines up with the contact lines of a helical gear pair. A given lead or involute modification now has a more complex and potentially less effective influence on the transmission error. Arguing that 2D modifications are not optimum for helical gears, a number of investigators proposed another class of modifications exclusively for helical gears [15-18]. Such three-dimensional (3D) modifications are illustrated in Fig. 1(b). Here, again the modifications are applied by removing material from the perfect involute profile. As evident from Fig. 1(b), 3D modifications can be designed to align with the contact lines of the helical gear. In each corner, a modification starts from a line joining two points at a roll angle β and a lead position λ. It varies linearly or quadratically as it reaches to a magnitude b in the corner. The modifications parallel to the contact line are often called as *bias-in* (modifications in corners 1 and 3 in Fig. 1(b)) and the modifications that are somewhat perpendicular to the contact line are often called as *bias-out* (corners 2 and 4) in gear terminology. The parameter set that defines the 3D modifications of gear i is given as

$$P_{3D}^{i} \in \{b_1^i, \beta_1^i, \lambda_1^i, b_2^i, \beta_2^i, \lambda_2^i, b_3^i, \beta_3^i, \lambda_3^i, b_4^i, \beta_4^i, \lambda_4^i\} \quad (4)$$

resulting in a 24 parameter set $P_{3D} \in P_{3D}^{p} \cup P_{3D}^{g}$ for a pair formed by gears p and g.

1.2 Objectives and Scope

Although both 2D and 3D modifications (especially the 2D ones) have been used extensively in real-life gear applications, the results have been often mixed mainly since the determination of the modification parameters were based on simplified estimates, trial-and-error or past field experiences. Although, tooth surface modifications can be very beneficial in reducing gear vibration excitation, their improper use can make the things even worse. One main objective of this study is to propose a contact mechanics model of a spur or helical gear pair for an accurate prediction of loaded transmission error. An experimental study will be outlined for measurement of loaded transmission error under quasi-static conditions. The model predictions will be validated through a comparison to the experimental data. The model will be used to systematically investigate the sensitivity of each parameter defining both 2D and 3D modifications on the Fourier harmonics of the loaded transmission error of a helical gear pair. Results of 2D and 2D modifications will be compared to identify their characteristic differences.

2 Model and Validation

2.1 Gear Contact Model

As described earlier, any prediction of the static transmission error involves not only the geometric deviations but also the deformations. An accurate static elastic model of system is required for this purpose. Yet the contact problem of helical gears is a rather challenging task. A gear pair contact has a number of unique characteristic features that makes the use of conventional finite element method (FEM) very inefficient and in many aspects inaccurate. First of all, the width of a typical helical gear contact zone is at least an order of magnitude smaller than the other gear dimensions requiring a very refined mesh near the contact zone when conventional FEM is used. As contact zone travels over the tooth profile surfaces, this fine mesh must follow it resulting in a refined mesh over the entire tooth surfaces. The computational time required by FEM to accommodate such a fine mesh is often overwhelming. In addition, the level of geometric accuracy required from a gear contact analysis is so high that a conventional FEM approach fails to deliver. Finally, there are major difficulties with conventional FEM in generating an optimal 3D mesh that is capable of modeling the stress gradients in the critical regions, especially at the tooth root, while minimizing the total number of degrees of freedom of the entire model.

The contact model employed in this study [19,20] overcomes such difficulties by using FEM and surface integral methods in conjunction. A brief description of the salient features of the model as applied to a helical gear pair is given here as the details of the model formulation can be found in papers by Vijayakar [19, 20].

The first task in gear contact analysis is determining the areas that will be in contact at any given position when the gear pair is subject to a torque. A computational grid that is set up in the contact zone of the gears obtained by dividing the entire face width of each gear into $(2N+1)$ slices. A surface point on the mid-plane of each slice of gear p that is closest to the surface of gear g is determined. This selection is carried out using the undeformed geometry. A set of $(2M+1)$ grid cells is set up centered around this closest point of each slice. Values of $M=5$ and $N=20$ are used in this study. The actual dimension of the grid cells in the profile direction is also selected such that the entire contact zone is about 30 to 40 percent smaller that the grid area defined.

One of the main features of the model used here [19,20] is the combined use of surface integral and finite element formulations. The inward normal component of the displacement vector $u(\mathbf{r}_{ij};\mathbf{r})$ of a field point $\mathbf{r}$ due to a normal load applied at a surface grid point $\mathbf{r}_{ij}$ is expressed as

$$u(\mathbf{r}_{ij};\mathbf{r}) = [u^{(si)}(\mathbf{r}_{ij};\mathbf{r}) - u^{(si)}(\mathbf{r}_{ij};\mathbf{q})] + u^{(fe)}(\mathbf{r}_{ij};\mathbf{q}) \quad (5)$$

where superscripts (*si*) and (*fe*) indicate the terms calculated by using the surface integral and finite element formulations, respectively. The term within the brackets represent the deformation of the point $\mathbf{r}$ with respect to the reference point $\mathbf{q}$ that is better estimated by local deformation field on the Bousinesq half space solution than finite elements. The last term on the right hand side is not influenced much by the local effects at the surface, and hence, it can be computed accurately by FEM. A matching interface parallel to the contact surface is

chosen at a depth on half a finite element dimension below the contact surface to build a compliance matrix that is solved by using a revised Simplex algorithm.

In terms of finite element representation of the contacting gear bodies, the displacements and coordinates within a finite element are approximated by separate sets of shape functions. In order to achieve maximum resolution in the root regions, full cubic elements with 16 nodes are used. For coordinate interpolation, the shape functions are such that interior elements are conventional four-noded, linear, two-dimensional elements.

A helical gear pair whose design parameters defined in Table 1 will be used as an example system. Figure 2 shows the 3D contact mechanics model obtained by using the model described above. Here only seven-tooth segments of both gears are included in the model. As the main focus of this study is on the prediction of the loaded transmission error $\varepsilon(t)$, the analysis is performed at 16 position angles defining a complete gear mesh cycle, $\varepsilon(t)$ is predicted as a function of position (or time), and Fourier coefficients are computed to obtain the harmonic content of the transmission error excitation.

2.2 Validation of the Model

Before any extensive parametric studies can be performed, the transmission error predictions of the computational model must be validated though controlled laboratory experiments. In order to measure the loaded transmission error under static conditions, a power-circulation type of gear test machine shown in Fig. 3 was used. Details of the test machine can be found in earlier papers by the second author [4, 6].

Since rather small angular vibration amplitudes constitute the transmission error, a pair of high precision optical encoders (18,000 pulse/revolution, Heidenhain model: RON 287) are employed for measurement of rotational angles θ of each gear. A pair of signal conditioners (Heidenhain model: IBV 600) are used to convert the harmonic encoder signals into TTL square-wave pulse trains with distinct rising and falling edges. Figure 3 illustrates the instrumentation that includes the optical encoders, signal conditioners, and a high-speed data analyzer. The analyzer software uses a pulse timing technique similar to the ones used previously [21,22] that internally compares the rising edges of each pulse train against a common 100 MHz timer. Combined with the gear pair radii and tooth count input into the analyzer, the timing of the pulses is used to calculate the velocity of each gear. Since the high frequency timer is common to both pulse trains, data of one gear is subtracted from the other to yield $d\varepsilon / dt$ that is integrated numerically to obtain $\varepsilon(t)$.

2.3 Comparison with Model Predictions

Two pairs of precision ground spur gears one of which shown in Fig. 4 are used here for a validation of the model. Although both test gear pairs have the same basic gear parameters listed in Table 1, they differ in terms of their tooth profile modifications. The first spur test gear pair chosen has a rather short profile tip modification starting at a roll angle of $\alpha_t = 23.6^\circ$ (far above the pitch point at $\alpha = 20.9^\circ$ degrees) and the second pair has its tip modification start at the pitch point $\alpha_t = 20.9^\circ$. Gears of both pairs have tip relief magnitudes $a_t = 10\ \mu m$ and a symmetric, parabolic lead modification of $h = 4\ \mu m$.

Tests performed with both gear pairs covering a torque range of 0 to 300 *Nm* at an angular velocity of 100 *rpm* such that no dynamic effects are present. The same gear pairs are simulated by using the model shown in Fig. 2, and the results are compared in Fig. 5. Figure 5(a) compares measured $\varepsilon(t)$ time histories of the first test gear pair with predicted ones for two complete mesh cycles at different load levels. The same scale is used for each $\varepsilon(t)$ in vertical axis except the mean values are shifted in order to be able to display them on the same figure in the form of a *Harris Chart* [14]. A good qualitative and quantitative agreement is evident in Fig. 5(a) regardless of *T*. The variation of $\varepsilon(t)$ is virtually eliminated at a *design load* of $T = T_d \approx 50$ *Nm* for this gear pair. The comparisons for the second test gear pair is shown in Fig. 5(b). Now $T_d \approx 200$ *Nm*. Again, the measured $\varepsilon(t)$ are in good agreement with the predictions. It can be stated from Fig. 5 that the model predictions are reasonably accurate for all practical engineering purposes. It is especially encouraging that the model predicts the same T_d values as the measurements suggesting that the optimum modifications defined using this model should be valid.

3 Parametric Studies

3.1 2D Tooth Surface Modifications

Parameters defining 2D tooth profile modifications which are described in Fig. 1(a) and equation (3) can be classified in three groups, namely tip, root and lead modifications. A parametric study that includes all 10 parameters defining the most general form of 2D modifications is not feasible. Since the example helical gear pair used in this parametric study as defined in Table 1 is formed by two identical (except their hand) helical gears, without loosing generality, same type and amount of modifications will be applied to both gears here. Accordingly, the parameters in each set, P_{2D}^p and P_{2D}^g, will have identical values reducing the total number of parameters to 5. Further, profile modifications will be applied only at the tip of both mating gears simply since a root modification on the teeth of a gear impacts $\varepsilon(t)$ in a very similar fashion as a tip modification of same type and amount on the mating gear tooth surface. Hence, parameter sub-set that is employed here is reduced to $P_{2D} \in \{a_t, \alpha_t, h\}$ where $a_t = a_t^p = a_t^g$, $\alpha_t = \alpha_t^p = \alpha_t^g$ and $h = h^p = h^g$.

First, the magnitude a_t of a linear tip relief applied is varied to quantify its influence on $\varepsilon(t)$. The other two parameters are kept constant at $\alpha_t = 22.2^\circ$ and $h = 2\mu m$. The predicted $\varepsilon(t)$ time histories are analyzed to obtain Fourier harmonics of $\varepsilon(t)$. The three dimensional plot of Fig. 6(a) demonstrates the combined effect of torque transmitted T and a_t on the fundamental (gear mesh) harmonic amplitude of $\varepsilon(t)$, A_1. Here, at a given a_t value, A_1 follows a characteristic "V-shape" profile as T is varied, reaching its minimum value at its design load $T = T_d$. For instance, a gear pair having a linear tip relief of $a_t = 5\mu m$ exhibits a minimum A_1 value at $T = 200\,Nm$ suggesting that this particular

modification would be optimum for the example gear pair when operated at $T = 200\,Nm$. Changing T in either direction from this particular value increases A_1. This is also evident from the predicted time histories $\varepsilon(t)$ shown in Fig. 7 for $a_t = 10\,\mu m$ at various levels of T. A higher T value simply produces a larger amount of tooth deflection requiring a larger modification to compensate it. Following the valley in Fig. 6(a), T_d increases linearly with increasing a_t. The same behavior was reported previously for spur gears [9,13,23]. As shown in Fig. 8(a), the variation of the transmission error first harmonic amplitude A_2 with varying T and a_t follows the same pattern as that of A_1 in Fig. 6(a) except A_2 amplitudes are significantly lower. Here, A_2 amplitudes become significant only at very high torque values.

Next, starting roll angle α_t of the linear tip modification in profile direction is varied while other two parameters are kept constant at $a_t = 10\,\mu m$ and $h = 2\,\mu m$. Combined influence of α_t and T on A_1 and A_2 amplitudes are shown in Figures 6(b) and 8(b), respectively. In Figure 6(b), as α_t is changed within the range of 17 to 27 degrees (the pitch point is at 20.9 degrees), T_d is first increases with α_t up to say $\alpha_t = 25^\circ$, beyond which it declines. At certain torque values, more than one T_d value becomes possible as this trajectory is crossed twice. For instance, at $T = 350\,Nm$, a gear pair having either one of $\alpha_t = 22^\circ$ or $\alpha_t = 26^\circ$ could be considered as optimum. One physical explanation why T_d starts reducing at higher values of α_t is that, as the starting point of the modification approaches closer to tip of the tooth, $\varepsilon(t)$ must take a shape similar to that of an unmodified gear pair. When α_t reaches the tip, the teeth are essentially unmodified, hence $T_d = 0$. Referring to Fig. 8(b), the variation of the first harmonic amplitude A_2 appears to follow the same trend as that of A_1 but the magnitude of A_2 is again considerably lower than A_1.

Finally, the amount of lead crown h illustrated in Fig. 1(b) is varied, given $a_t = 10\,\mu m$ and $\alpha_t = 22.2^\circ$. In Fig. 6(c), A_1 is plotted as a function of h and T. Here, A_1 again follows "V-shape" profile similar to Fig. 6(a) as T of a gear pair having a certain h is varied. The design load T_d is at the lower end of the torque range when $h = 0$ and increases with h on a trajectory defined by the valley of Fig. 6(c). As shown in Figure 8(c), the effect on h on A_2 is again very similar that of A_1, A_2 amplitudes becoming significant only at higher values of h and T.

In summary, $\varepsilon(t)$ is equally sensitive to all three parameters investigated above, a_t, α_t and h, making possible to define an optimum linear profile modification in more than one way. When a quadratic modification as shown in Fig. 1(a) is used in place of a linear modification, the overall sensitivity to these parameters remain relatively unchanged. For instance, the same conditions defining Fig. 6(a) are considered in Fig. 9 expect quadratic tip modifications are used in place of linear modifications. A comparison of Figures 6(a) and 9 suggest that the differences are minute, making Fig. 6 to 8 applicable for quadratic modifications as well for practical engineering purposes.

3.2 3D Tooth Surface Modifications

Referring to the 3D modification parameters defined in Fig. 1(b), corners 1, 2, 3 and 4 of gear *p* meshes with corners 3, 4, 1 and 2 of gear *g*, respectively. Again considering the case when the modifications applied to each gear in the pair are identical, parameter set defining 3D modifications can be reduced to 12 as the corresponding parameter included in each set P_{3D}^p and P_{3D}^g become equal, $b_i^p = b_i^g$, $\beta_i^p = \beta_i^g$ and $\lambda_i^p = \lambda_i^g$ ($i = 1\,to\,4$).

As the simplest example of bias-in type 3D modifications, consider the case with modifications only on the first corner of both gears as the other three corners are unmodified. First, the magnitude of the modification at the corner $b_1^p = b_1^g = b_1^i$ is varied with the other two parameters kept the same at $\beta_1^p = \beta_1^g = 15^\circ$ and $\lambda_1^p = \lambda_1^g = 20\,mm$. Combined influence of b_1^i and T on the fundamental harmonic A_1 of $\varepsilon(t)$ is shown in Fig. 10(a). Again, at any given b_1^i value, A_1 follows a V-shaped profile as T is changed similar to the influence of 2D modification parameter a_t shown earlier in Fig. 6(a). The design load T_d is at 150 Nm for $b_1^i = 2\,\mu m$ and at 350 Nm for $b_1^i = 5\,\mu m$. Although the dependence on the value of T is still evident, the overall A_1 amplitudes are somewhat lower and the changes in A_1 with T are less drastic when compared to Fig. 6(a). This suggests that 3D modifications could result in quieter gear sets in application when the operating torque range is wider as it is the case in most automotive and rotorcraft applications.

Next, the starting point of the bias-in modifications in involute direction $\beta_1^p = \beta_1^g = \beta_1^i$ is varied between roll angles of 15 and 25 degrees covering a wide range around the pitch point (20.9 degrees) as shown in Fig. 10(b). The other two parameters are maintained at $b_1^p = b_1^g = 5\,\mu m$ and $\lambda_1^p = \lambda_1^g = 20\,mm$. A 3D plot shown in Fig. 12(b) within the same range of T demonstrates the effect of β_1^i on A_1 that is qualitatively similar to Fig. 6(b) except now the sensitivity of A_1 to β_1^i is considerably less. The amplitudes of A_1 are rather low for a large range below $\beta_1^i = 23^\circ$ regardless of T.

As a final example of bias-in modifications, the starting position in lead direction $\lambda_1^p = \lambda_1^g = \lambda_1^i$ is varied with other two parameters kept the same at $\beta_1^p = \beta_1^g = 15^\circ$ and $b_1^p = b_1^g = 10\,\mu m$. Corners 2, 3 and 4 are again unmodified. Combined influence of λ_1^i and T on A_1 shown in Fig. 10(c) follows a similar pattern as Fig. 6(c), but slightly less sensitive than h.

Two separate cases are selected to demonstrate the influence of bias-out modifications on $\varepsilon(t)$. Corner 2 of each gear is modified in order to obtain a bias-out effect as other three corners on each gear profiles are left unmodified. First, the amount of modification $b_2^p = b_2^p = b_2^i$ is varied with $\beta_2^p = \beta_2^g = 15^\circ$ and $\lambda_2^p = \lambda_2^g = 20\,mm$. In Fig. 11(a), the influence of b_2^i on A_1 is shown. Similarly, the influence of $\lambda_2^p = \lambda_2^g = \lambda_2^i$ is illustrated in Fig. 11(b) with $\beta_2^p = \beta_2^g = 15^\circ$ and $b_2^p = b_2^g = 10\,\mu m$. Results for both cases suggest that A_1 increases with increasing with b_2^i or λ_2^i regardless of the value of T having its lowest value at $b_2^i = 0$ and $\lambda_2^i = 5\ mm$. Therefore, it can be suggested from Fig. 11 that bias-out modifications, when applied alone, are detrimental to $\varepsilon(t)$.

As a final case, consider a gear pair with bias in modifications $b_1^p = b_1^g = 10\,\mu m$, $\beta_1^p = \beta_1^g = 20.8^\circ$ and $\lambda_1^p = \lambda_1^g = 10\,mm$. In addition, a bias-out modification of fixed starting points $\beta_2^p = \beta_2^g = 20.8^\circ$ and $\lambda_2^p = \lambda_2^g = 10\,mm$, but of variable magnitude $b_2^p = b_2^g = b_2^i$ is applied. In Fig. 12, the influence of b_2^i on A_1 is shown together with a schematic of the modifications applied. Here, $T_d = 700\,Nm$ for $b_2^i = 0$ (only bias-in modifications) and T_d reduces linearly as b_2^i is increased. This suggests that bias-out modifications, although they are not beneficial when used alone, offer added flexibility for optimizing modifications for reduced $\varepsilon(t)$.

4 Conclusions

In this study, a nonlinear finite element contact mechanics model of a parallel axis gear pair was employed to study the impact of intentional tooth flank modifications on the static motion transmission error of the gear pair. An experimental study was performed to demonstrate the accuracy of the predictions the model. The model was used to investigate the impact of both conventional 2D and 3D tooth flank modifications on the transmission error excitation. In case of 2D modifications, a parameter set that included the magnitude, extent, and type (both linear or quadratic) of involute tip modifications and lead crown. For 3D modifications, parameters defining both bias-in and bias-out type of modifications were included. The combined influence of modification parameters and load transmitted on the resultant transmission error excitation is quantified.

It was demonstrated that both types of modifications can be designed to minimize the static transmission error excitation at a given fixed design load. Neither modification scheme was found to eliminate the influence the applied load on the static transmission error amplitude, while the 3D modifications were found to be better on this aspect. Our ongoing work on this subject matter focused on the changes on gear stresses and gear life as a function of the same gear tooth modifications [24]. In addition, the dynamic consequences of helical gear tooth modifications are also being investigated experimentally and theoretically.

Acknowledgments

We thank Dr. S. Vijayakar of Advanced Numerical Solutions Inc. for making the gear contact analysis package *CAPP* available and for his technical guidance. We also thank Mr. D. Hoying of M&M Precision Systems Corp. for providing some of the instrumentation used in the experimental study. Finally, we thank Dr. G. W. Blankenship of Superior Controls for making the Transmission Error Measurement System *TEMS* available.

References

[1] Ozguven, H. N. and Houser, D. R., 1988, "Mathematical Models Used in Gear Dynamics – a Review," *Journal of Sound and Vibration,* **121**, pp. 383-411.

[2] Kahraman, A. and Singh, R., 1990, "Nonlinear Dynamics of a Spur Gear Pair," *Journal of Sound and Vibration,* **142**, pp. 49-75.

[3] Blankenship, G. W. and Singh, R., 1995, "Analytical Solutions for Modulation Sidebands Associated with a Class of Mechanical Systems," *Journal of Sound and Vibration* **179**, pp. 13-36.

[4] Blankenship, G. W. and Kahraman, A., 1995, "Steady state forced response of a mechanical oscillator with combined parametric excitation and clearance non-linearity," *Journal of Sound and Vibration,* **185**, pp. 743-765.

[5] Umezawa, K., Sato, T, and Ishikawa, J., 1984, "Simulation of Rotational Vibration of Spur Gears," *Bulletin of Japan Society of Mechanical Engineers,* **38**, pp. 102-109.

[6] Kahraman, A., and Blankenship, G. W., 1997, "Experiments on Nonlinear Dynamic Behavior of an Oscillator with Clearance and Periodically Time-varying Parameters, *ASME Transactions*, *Journal of Applied Mechanics,* **64**, pp. 217-226.

[7] Padmanabhan, C. and Singh, R., 1995, "Analysis of Periodically Forced Hill's Oscillator with Application to a Gear System," *Journal of Sound and Vibration,* **184**, pp. 769-799.

[8] Kiyono, S., Aida, T., and Fujii, Y., 1978 "Vibration of Helical Gears: Part 2 – Experimental Validation," *Bulletin of Japan Society of Mechanical Engineers,* **2**, pp. 923-930.

[9] Gregory, R. W., Harris, S. L. and Munro, R. G., 1963, "Dynamic Behavior of Spur Gears," *Proceedings of the Institute of Mechanical Engineers,* **178**, pp. 207-225.

[10] Ozguven, H. N. and Houser, D. R., 1988, "Dynamic Analysis of High Speed Gears by Using Loaded Static Transmission Error," *Journal of Sound and Vibration,* **125**, pp. 71-83.

[11] Parker, R. G, Vijayakar, S. M., Imajo, T., 2000, "Nonlinear Dynamic Response of a Spur Gear Pair: Modeling and Experimental Comparisons," *Journal of Sound and Vibration,* **237**, pp. 435-445.

[12] Kahraman, A. and Blankenship, G. W., 1999, "Effect of Involute Contact Ratio on Spur Gear Dynamics," *ASME Transactions*, *Journal of Mechanical Design,* **121**, pp. 112-118.

[13] Kahraman, A. and Blankenship, G. W., 1999, "Effect of Involute Tip Relief on Dynamic Response of Spur Gear Pairs," *ASME Transactions*, *Journal of Mechanical Design,* **121**, pp. 313-315.

[14] Harris, S. L., 1958, "Dynamic Loads on the Teeth of Spur Gears," *Proceedings of the Institute of Mechanical Engineers*, pp. 87-112.

[15] Umezawa, K., Wang, S., Houjoh, H. and Matsumura, S., 1998, "Dynamics of Gear Pairs with Bias Modifications," *JSME Transactions,* pp. 1414-1420.

[16] Saiki, K. and Watanabe, T., 2000, "Transmission Error Analysis of Helical Gears for any Load Condition," *Proceedings of 8th International Power Transmission and Gearing Conference*, PTG-14421.

[17] Umeyama, M., Kato, M., and Inoue, K., 1998, "Effects of Gear Dimensions and Tooth Surface Modifications on the Loaded Transmission Error of a Helical Gear Pair," *ASME Journal of Mechanical Design,* **120,** pp. 119-125.

[18] Umezawa, K., 1999, "Low Vibration Design on a Helical Gear Pair," *AGMA Fall Annual Meeting. Cincinnati.*

[19] Vijayakar, S., 1991, "A Combined Surface Integral and Finite Element Solution for a Three-dimensional Contact Problem," *International Journal for Numerical Methods in Engineering*, **31**, pp. 525-545.

[20] Vijayakar, S. M., Busby, H. R., and Houser, D. R., 1987, "Finite Element Analysis of Quasi-prismatic Bodies Using Chebyshev Polynomials," *International Journal for Numerical Methods in Engineering*, **24**, pp. 1461-1477.

[21] Remond, D., 1998, "Practical Performances of High-Speed Measurement of Gear Transmission Error or Torsional Vibrations with Optical Encoders," *Meas. Sci. Technology,* **9**, pp. 347-353.

[22] Bard, C., Remond, D., and Play, D., 1994, "New Transmission Error Measurement for Heavy Load Gears," *International Gearing Conference*. Newcastle upon Tyne, England, pp. 393-399.

[23] Munro, R. G., 1962, "Dynamic Behavior of Spur Gear Pairs," Ph.D. Dissertation, University of Cambridge, England.

[24] Wagaj, P. and Kahraman, A., 2002. "Impact of Profile Modifications Helical Gear Contact and Bending Stresses," in print, *ASME Journal of Mechanical Design*.

Table 1
Basic design parameters of the example gear pairs used (all dimensions are in mm unless specified)

Number of teeth	50
Transverse module	3.0
Face width	20.0
Transverse Pressure angle (deg.)	20
Helix angle (deg.)	0.0 (spur) 25.232 (helical)
Center Distance	150.0
Major diameter	156.0
Base diameter	140.954
Root Diameter	140.68
Circular tooth thickness	4.64

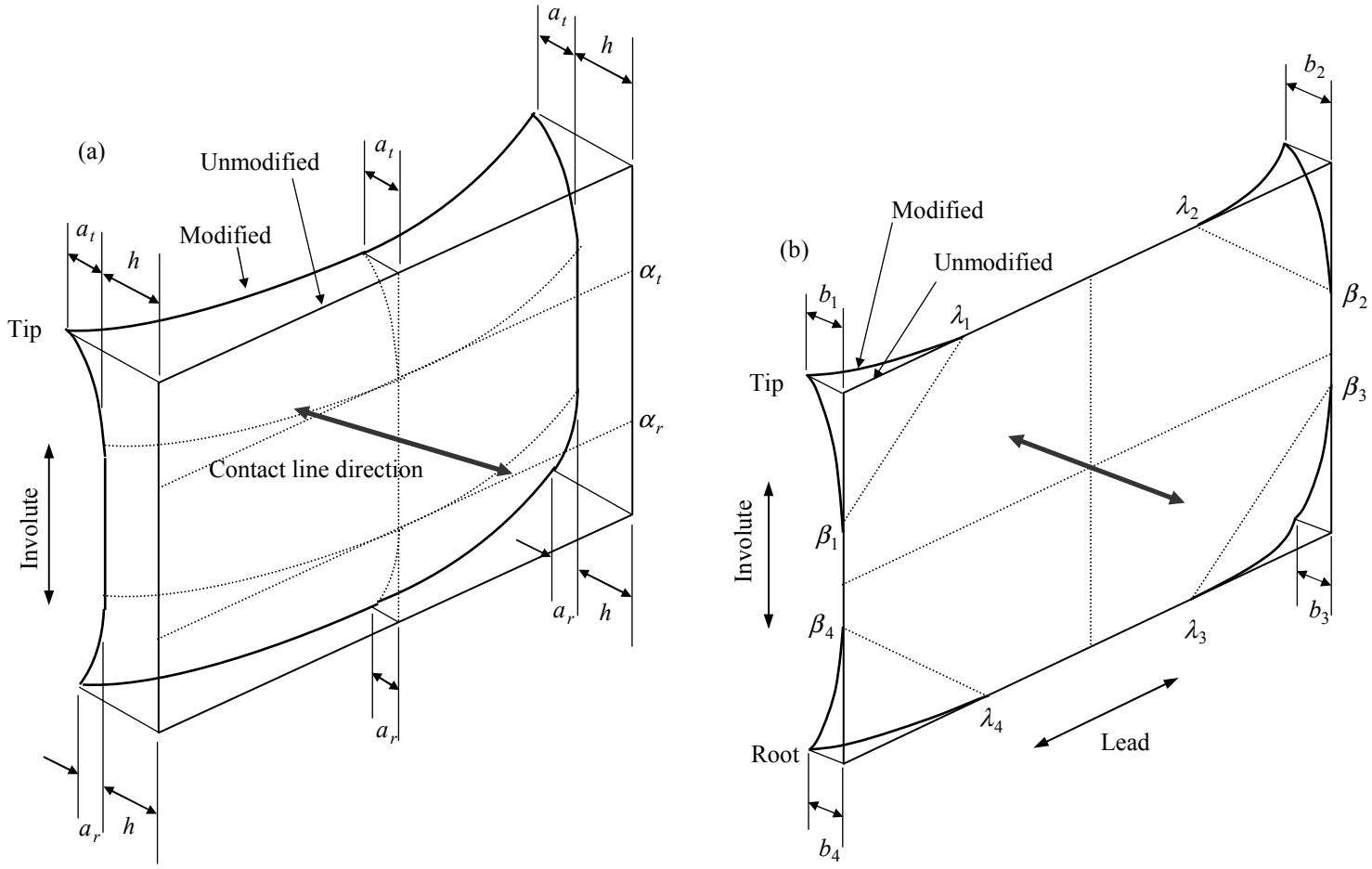

Fig. 1 Definition of (a) 2D and (b) 3D tooth surface modification parameters.

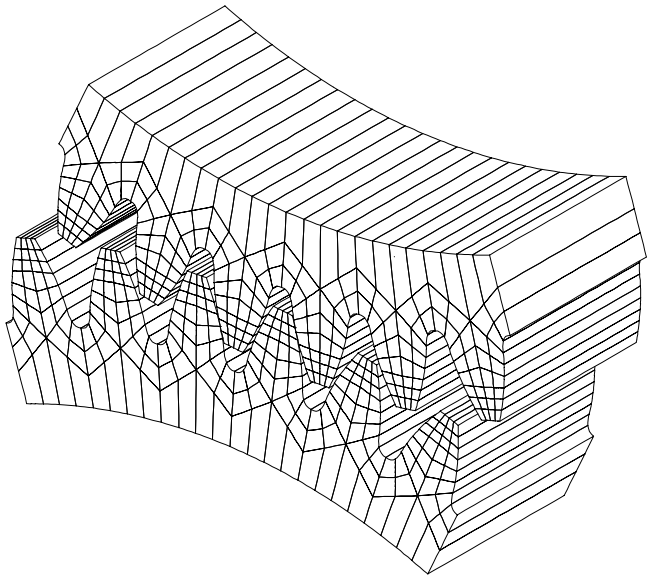

Fig. 2 Contact model of the example helical gear pair.

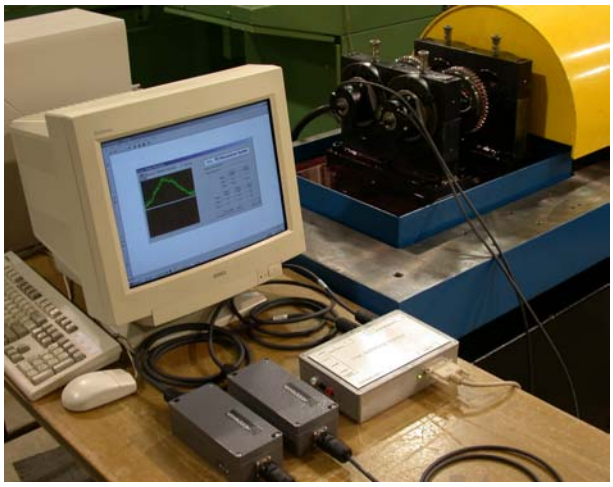

Fig. 3 Transmission error test machine with optical encoders, signal conditioners and the analyzer.

Fig. 4 An example spur test gear pair.

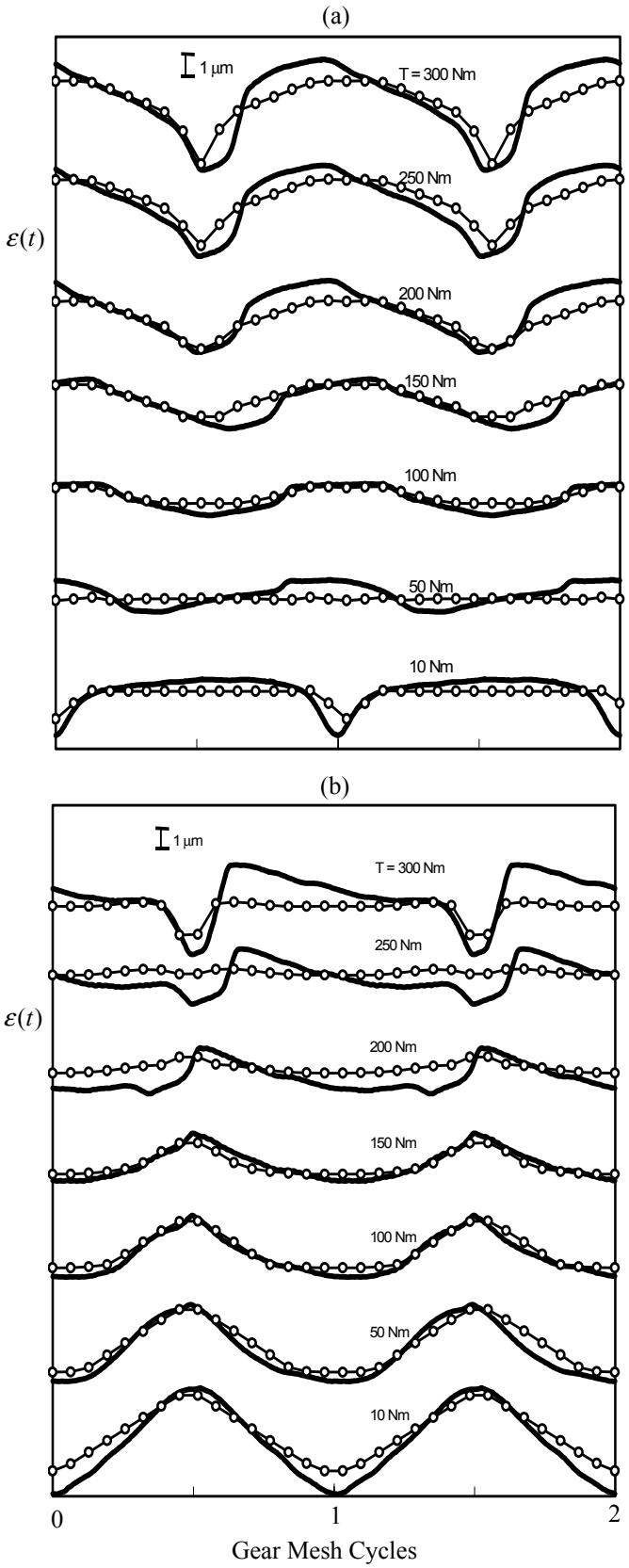

Fig. 5 Measured and predicted $\varepsilon(t)$ of test gear pair under different torque levels. (a) $a_t = 10\,\mu m$, $\alpha_t = 23.6^\circ$, $h = 4\,\mu m$, and (b) $a_t = 10\,\mu m$, $\alpha_t = 20.9^\circ$, $h = 4\,\mu m$. (——) Measurement, (—o—) prediction.

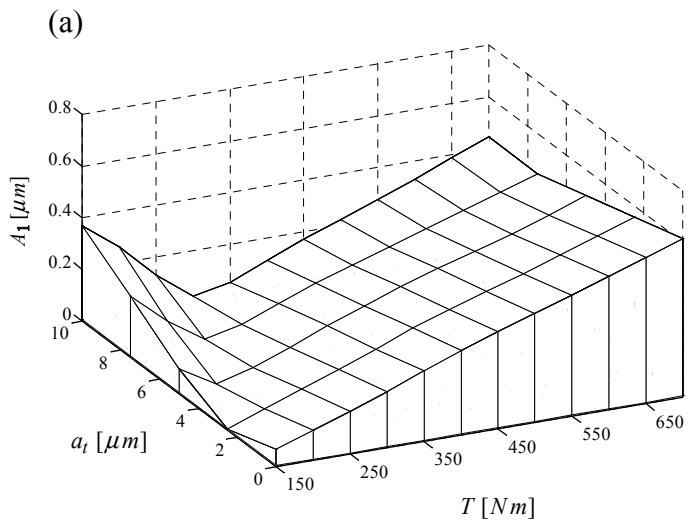

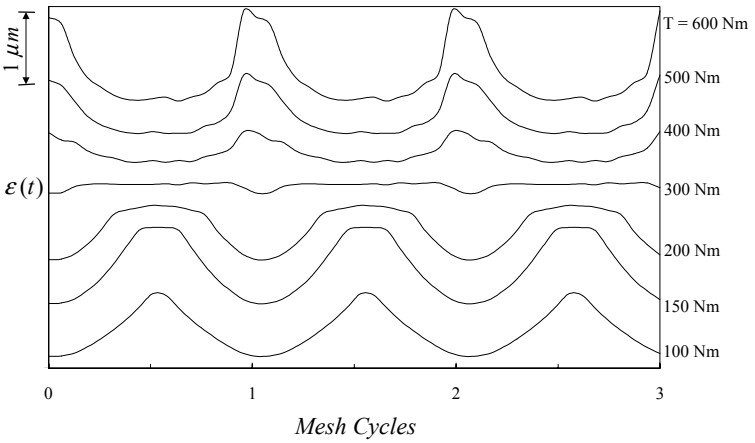

Fig. 7 Variation of predicted $\varepsilon(t)$ as a function of T; $a_t = 10\,\mu m$, $\alpha_t = 22.2^\circ$ and $h = 2\,\mu m$.

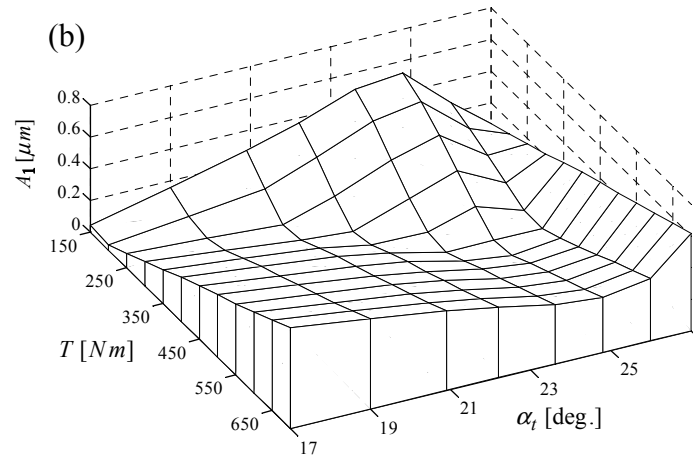

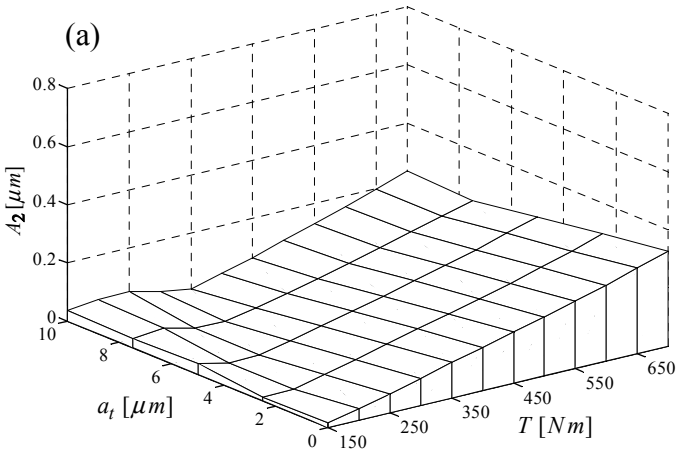

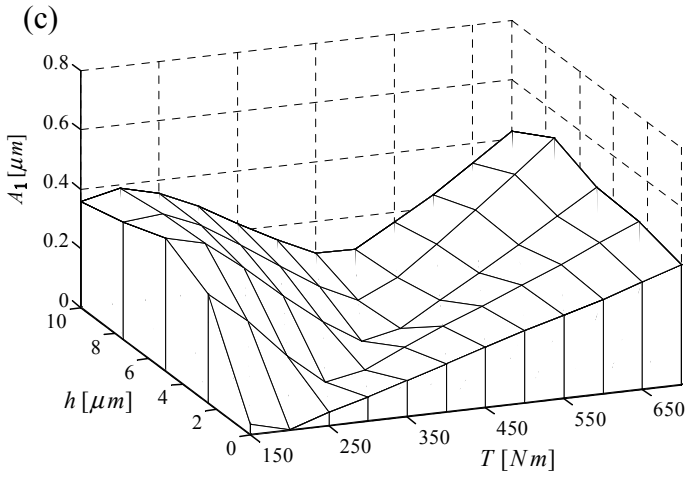

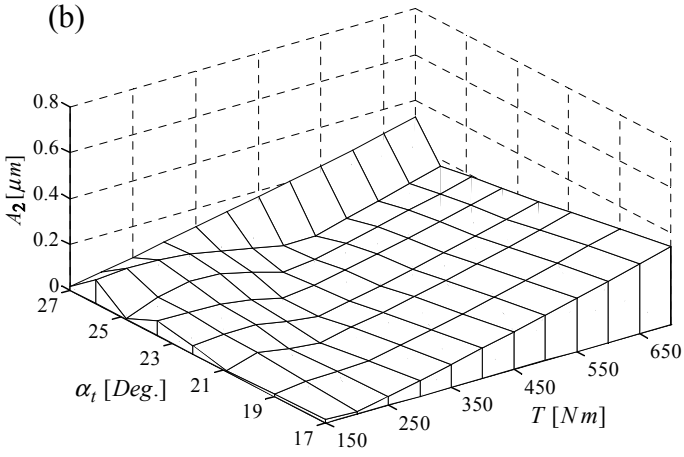

Fig. 6 Variation of A_1 with T and 2D linear tip modification parameters; (a) a_t: variable, $\alpha_t = 22.2^\circ$ and $h = 2\,\mu m$, (b) α_t: variable, $a_t = 10\mu m$ and $h = 2\,\mu m$, and (c) h: variable, $a_t = 10\mu m$ and $\alpha_t = 22.2^\circ$.

Fig. 8 Variation of A_2 with T and 2D linear tip modification parameters; (a) a_t: variable, $\alpha_t = 22.2^\circ$ and $h = 2\,\mu m$, (b) α_t: variable, $a_t = 10\mu m$ and $h = 2\,\mu m$, and (c) h: variable, $a_t = 10\mu m$ and $\alpha_t = 22.2^\circ$.

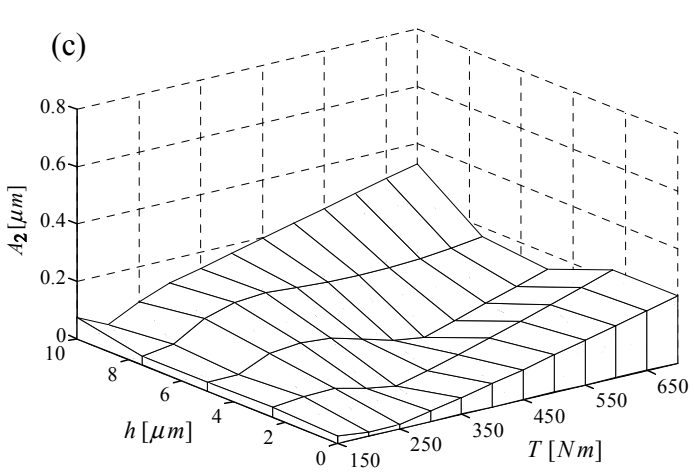

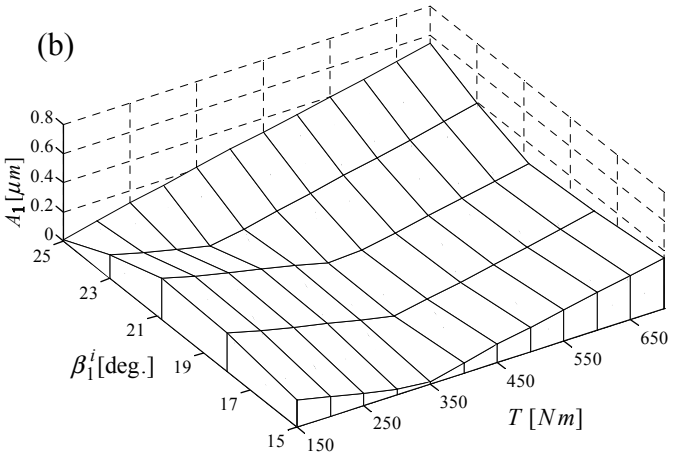

Fig. 8 Continued.

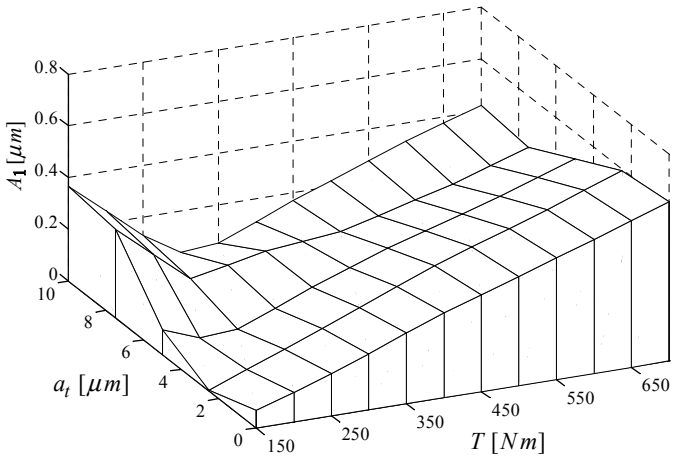

Fig. 9 Variation of A_1 with T and 2D quadratic tip modification magnitude a_t; $\alpha_t = 22.2^\circ$ and $h = 2\,\mu m$.

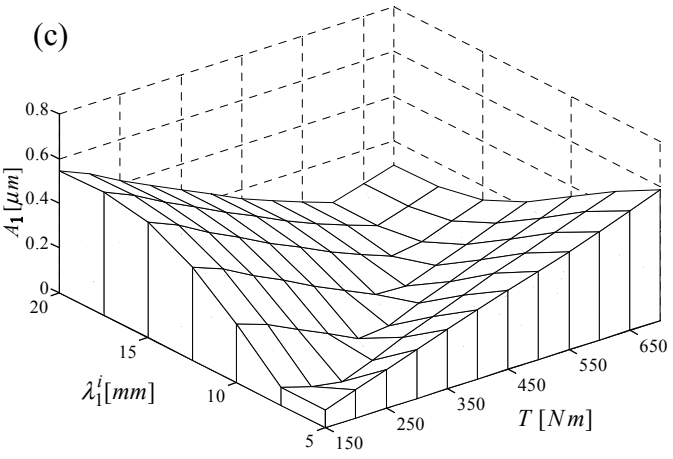

Fig. 10 Continued.

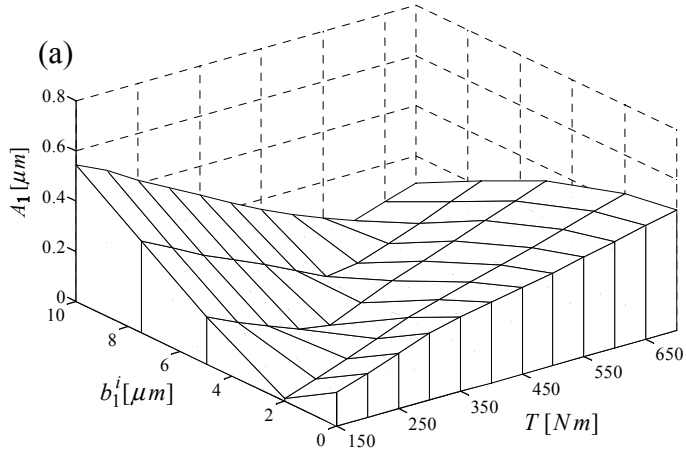

Fig. 10 Variation of A_1 with T and 3D bias-in modification parameters; (a) b_1^i: variable, $\beta_1^i = 15^\circ$ and $\lambda_1^i = 20\,mm$, (b) β_1^i: variable, $b_1^i = 5\,\mu m$ and $\lambda_1^i = 20\,mm$, and (c) λ_1^i: variable, $b_1^i = 10\,\mu m$ and $\beta_1^i = 15^\circ$.

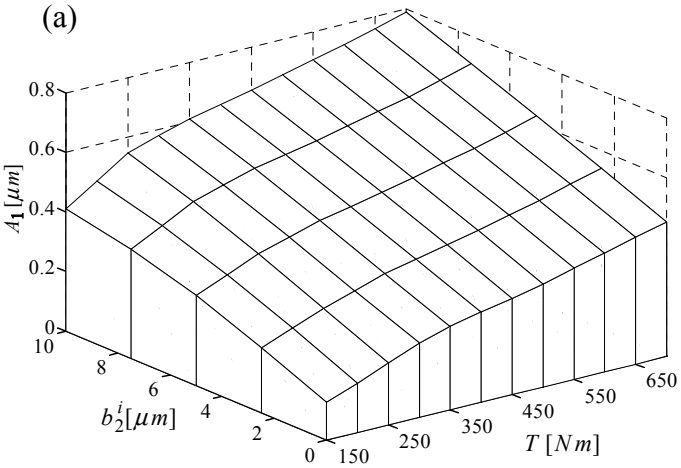

Fig. 11 Variation of A_1 with T and 3D bias-out modification parameters; (a) b_2^i: variable, $\beta_2^i = 15^\circ$ and $\lambda_2^i = 20\,mm$, and (b) λ_2^i: variable, $b_2^i = 10\,\mu m$ and $\beta_2^i = 15^\circ$.

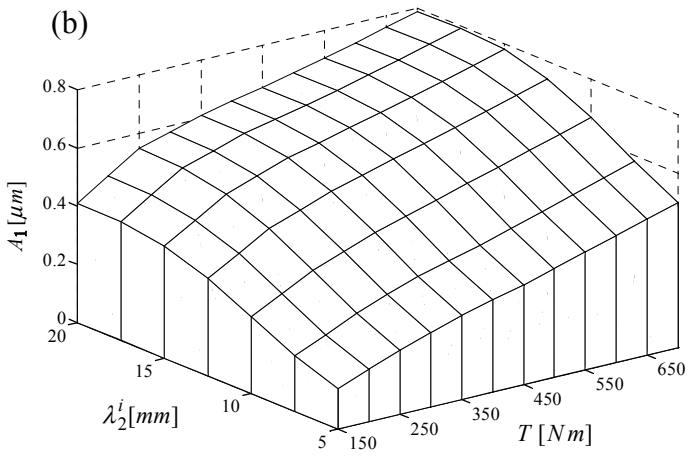

Fig. 11 Continued.

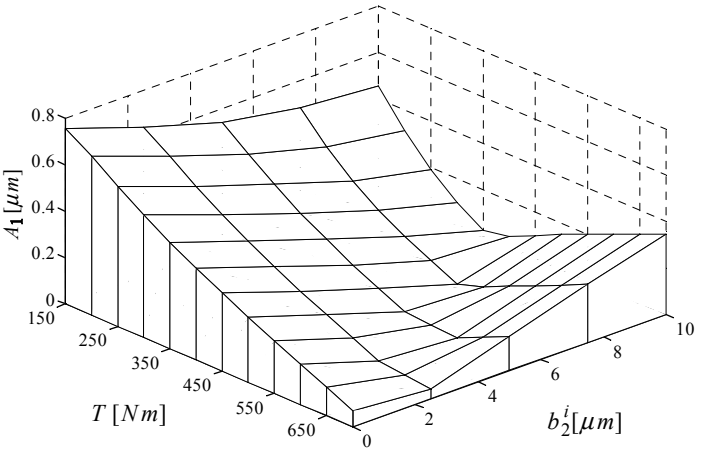

Fig. 12 Variation of A_1 with T and combined bias-in and bias-out modifications; b_2^i: variable, $b_1^{\ i} = 10\,\mu m$, $\beta_1^{\ i} = \beta_2^{\ i} = 20.8^\circ$, and $\lambda_1^i = \lambda_2^i = 10\,mm$.